RESEARCH ARTICLE

Sub-picosecond ballistic imaging of a liquid jet

Saïd Idlahcen · Claude Rozé · Loïc Méès ·
Thierry Girasole · Jean-Bernard Blaisot

Abstract A diesel jet visualisation based on an ultra-short light pulse and a time-resolved detection is proposed. An optical gate, consisting of a beta barium borate crystal, allows to separate ballistic, refractive and scattered light. An imaging pulse passes through the studied medium, while a gating pulse is used to open the gate. With this configuration, a spatial resolution of 10 μm and a temporal resolution of 270 fs are obtained. The gate duration is compatible with the typical dimensions of a liquid jet generated by a commercial automotive fuel injector. Preliminary results show that spatio-temporal diagrams of transmitted light through a spray may be acquired, showing clearly the separation between ballistic, refracted and scattered light.

1 Introduction

Optimal use of liquid fuel needs a perfect understanding of the liquid injection inside the combustion chamber and of its break-up into small droplets. High-pressure injection leads to complex structures in the near field of the nozzle, where the liquid column is degraded into droplets, liquid filaments, etc. Due to its turbid nature, this highly non-homogeneous medium is difficult to image accurately. Large efforts have been made to extract information on the spray structure by eliminating scattering light. X-ray absorption used by Kastengren et al. (2008) on a diesel injector provides measurements of the fuel mass. Nevertheless, the beam configuration of the X-ray source leads to the impossibility to obtain single-shot images. X-ray phase contrast technique (Moon et al. 2010) allows to obtain single-shot images, but is difficult to interpret and is hampered by the difficulty to operate in a pressure chamber, because X-rays are strongly attenuated by windows. Optical techniques are more versatile. The usual trend is to detect a signature of the light that has not been perturbed by multiple interactions with the liquid during its propagation through the spray. SLIPI (structured laser illumination planar imaging) consists in illuminating the spray with a spatially structured laser sheet, and detecting the light, which has kept this spatial signature (Kristensson et al. 2010; Berrocal et al. 2011; Leick et al. 2011). Ballistic imaging consists in using very short laser pulses and detecting the directly transmitted light or ballistic light, which keeps information on the structure of the spray. Time-gated imaging techniques have been proposed (Galland et al. 1995; Paciaroni et al. 2006; Linne et al. 2006; Schmidt et al. 2009; Idlahcen et al. 2009) to visualise the liquid core, despite the surrounding scattering droplets cloud. Ballistic imaging is particularly useful in the very near field of the injector nozzle, where the size of the spray is comparable to the size of a laser sheet and SLIPI technique is ineffective.

In the ideal case of the strongly scattering medium of very small particles (<2 μm) and a small detection acceptance angle (<5°), the light transmission consists of two components, a ballistic and a scattered one (Berrocal et al. 2009). As an illustration, Fig. 1 shows a typical transmitted light evolution in time (Calba et al. 2008). It corresponds to the transmission of a 100 fs pulse through a

S. Idlahcen · C. Rozé (✉) · T. Girasole · J.-B. Blaisot
UMR 6614-CORIA, CNRS, Université et INSA de Rouen,
BP12, Avenue de l'Université, 76801 Saint-Étienne du Rouvray
Cedex, France
e-mail: roze@coria.fr

L. Méès
CNRS, UMR 5509 LMFA, École centrale de Lyon, 36 avenue
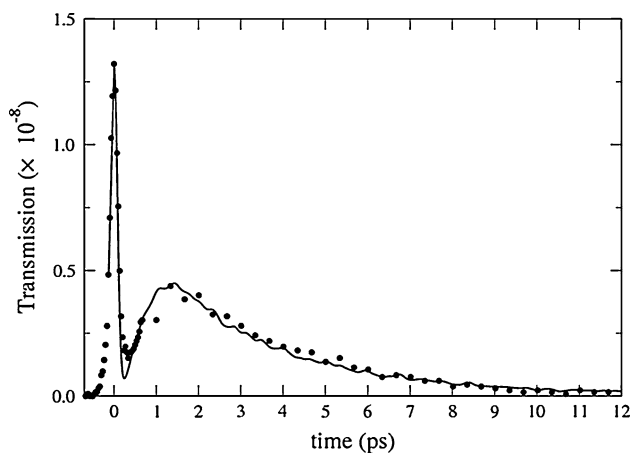Guy-de-Collongue, 69134 Écully Cedex, France

Fig. 1 Time-resolved transmission of a 100-fs light pulse through a glass particle suspension. Particle diameter is 1.8 μm, and optical depth is 18.16. Details of comparison between numerical (*solid line*) and experimental (*dots*) results can be found in Calba et al. (2008)

strongly scattering suspension of glass particles in water. The first peak corresponds to the ballistic photons, which have not interacted with the scatterers and constitute the first detected light. Scattered photons undergo multiple interactions, their trajectories are elongated and they are time delayed by a few picoseconds (second peak).

In the spray configuration, the droplets average diameter is close to 10 μm. Berrocal et al. (2009) performed numerical computations showing that for 5-μm droplets and a large detection acceptance angle (>5°), there is no more separation between a ballistic peak and the scattered pulse. Computations of pulse transmission through a large droplet (50 μm) cloud with a very small detection acceptance angle (<2°) have shown that the transmitted light is again separated into two contributions (Calba et al. 2006). The first one is a mixture of ballistic photons and diffracted light and the second one containing mainly the scattered light.

In any case, in time-resolved imaging techniques (ballistic imaging), an appropriate temporal selection of the transmitted light reduces the influence of the scattered photons. A shadowgraph of the liquid spray may then be obtained by limiting the scrambling effect of multiple scattering. A numerical demonstration of the contrast enhancement by using a time gate may be found in Sedarsky et al. (2011).

The efficiency of ballistic imaging has been demonstrated through a 3.5-mm-thick human breast tissue for an 8 ps time gate (Wang et al. 1991) and through a 5-mm spray with a 2 ps time gate (Schmidt et al. 2009). Scattered photons time delay clearly depends on the optical length of the probed medium. Reducing the time resolution in ballistic imaging technique is suitable to investigate smaller sprays. Furthermore, a shorter time gate could provide

additional information on the liquid core, based on the separation between refractive light and ballistic light. Such a separation between scattering modes (reflection/diffraction, refraction, etc.) has been investigated experimentally (Sbanski et al. 2000) and numerically (Méès et al. 2001) in single-scattering configurations and in a multiple-scattering configuration (Calba et al. 2006).

Near the injector nozzle, the liquid has not completely disintegrated into a cloud of droplets. At this stage, the liquid keeps memory of the injector hole and is nearly cylindrical. Nevertheless, hydrodynamic surface instabilities appear in this domain and will lead to jet atomisation further from the nozzle. Some photons experience refractions through the liquid jet and may be delayed by a typical time $\Delta t = \frac{\Delta n d}{c}$, where Δn is the difference between the refractive index of the liquid and the surrounding gas, d is the diameter of the jet and c is the speed of light in free space. Knowing that in automotive internal combustion engines, diameter of injection hole is about 200 μm, a temporal detection with a resolution of ≈ 300 fs is a minimum to discriminate refracted photons from ballistic ones in the case of a liquid core of a size similar to the diameter of the hole. Where the spray begins to break-up at the exit of the injector, refractive light can no more be discriminated with such a resolution, but some multiple scattered light may be eliminated by a temporal detection, leading to better images of the liquid core. To reach this aim, an ultra-short light pulse (duration of 100 fs) illuminates the liquid jet and a time-resolved image is recorded; thanks to an ultra-fast time gate and a single CCD camera.

No electronic device can achieve such an ultrafast detection and an optical gate must be used. Two kinds of optical gate may be found in the literature based on (1) an optical Kerr effect or (2) a second-harmonic generation (SHG) in a non-linear crystal. In the referenced papers, optical Kerr gate is obtained by inducing a temporary birefringence in a Kerr active liquid between two crossed polarisers (Galland et al. 1995; Paciaroni et al. 2006; Linne et al. 2006; Schmidt et al. 2009; Idlahcen et al. 2009). The temporal resolution of the gate is fixed by molecular reorientation time of the Kerr liquid and is of about 1 ps or longer. The second kind of optical gate has been used to obtain ballistic images and detect hidden objects in a turbid medium (Farsiu et al. 2007; Kuditcher et al. 2001; Abraham et al. 2000).

The aim of this paper is to study the potential of SHG crystal time gate to extract shape properties of the liquid core/structure in the near field of an injector. In Sect. 2, the experimental setup based on a SHG gate is described. In Sect. 3, temporal and spatial resolutions are presented. Glass fibre and examples of images of a diesel jet from a high pressure injector are presented in the last section.

2 Experimental setup

The principle of optical gating is to divide the laser pulse of wavelength 800 nm into two pulses: the imaging pulse crosses the spray, while the gating pulse is used to open the time gate and may be shifted in time by means of a delay line. The time gate consists of a beta barium borate (BBO) crystal, which has a quadratic nonlinearity. The imaging pulse and the gating pulse are incident on the crystal with an angle θ. First, collinear SHG occurs, so that light at wavelength 400 nm is generated along the direction of each pulse. When the two pulses overlap spatially and temporally on the crystal, non-collinear second-harmonic pulse is generated in direction $\vec{k}(2\omega) = \vec{k}_1(\omega) + \vec{k}_2(\omega)$, which is the intermediate direction between the two collinear second-harmonic pulses. The crystal orientation is adjusted by a rotation around a vertical axis, in order to obtain the best conversion efficiency. The SHG is quasi-instantaneous, so that the gate duration is only limited by the gating pulse duration and angle between the pulses.

The integration of the gate inside the complete experimental setup is shown on Fig. 2. A Ti/Sa amplified laser system (800 nm, 1 kHz, 1 mJ) generates constant 100-femtosecond pulses. The beam profile is approximately Gaussian with a 5-mm full width at half maximum (FWHM).
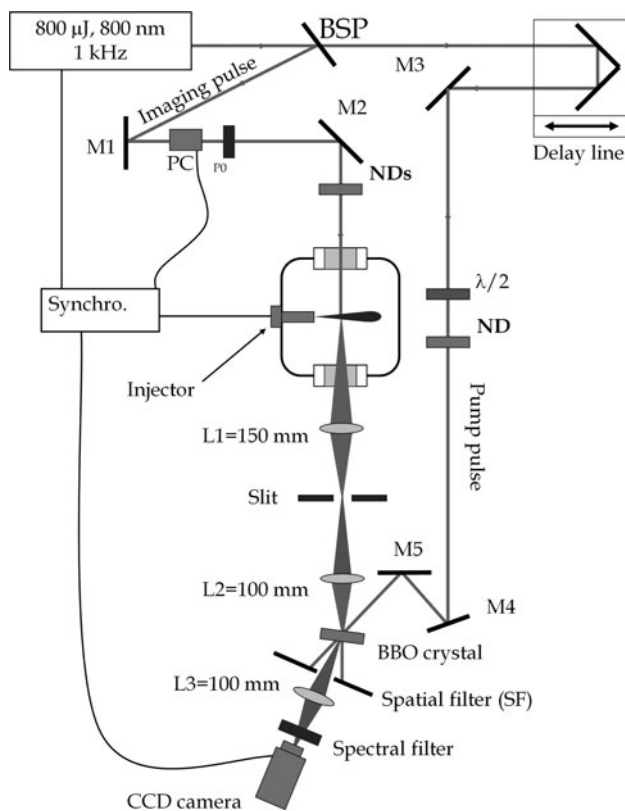

Fig. 2 Schematic diagram of experiment

The laser pulse is separated into two parts by means of a beam splitter (BSP), the imaging pulse and the gating pulse. The gating pulse passes through a delay line, a half-wave plate ($\lambda/2$) and a neutral density filter (ND), in order to adjust time delay, polarisation direction and intensity. The imaging pulse passes through a Pockels cell (PC) in order to decrease the repetition rate of the pulses down to 1 Hz (the spray repetition rate). A set of NDs is then used to adjust the lighting power. The imaging pulse next illuminates the spray injected in a chamber, equipped with glass windows. Imaging pulse and gating pulse are incident on a BBO crystal with the angle θ between them. Careful optical alignments are conducted to overlap the two beams in both spatial and temporal domains on the crystal. Non-collinear second-harmonic pulse is generated at half angle $\theta/2$ between the directions of the two pulses when and where they overlap. A time-gated second-harmonic image of the spray is then formed by means of a lens (L1, $f = 150$ mm). A vertical slit may be placed in the corresponding image plane, the use of which will be explained later. A second lens (L2, $f = 100$ mm) forms a second image of the spray on the BBO crystal. A third lens is used to record the non-collinear SHG on a CCD camera (Hamamatsu C9100). Light at fundamental wavelength (800 nm) is scattered and detected by the camera. This noise source is eliminated by a spectral filter placed between the BBO crystal and the CCD camera, increasing notably the signal-to-noise ratio. Collinear SHG from the imaging pulse and from the gating pulse may also be recorded by the camera. A spatial filter (SF) removed this unwanted light.

3 Time gate properties

3.1 Temporal resolution

In order to measure the temporal profile of the gate, the power of the SHG pulse at angle $\theta/2$ is measured for various delays between the imaging pulse and the gating pulse, without liquid jet. The result is shown on Fig. 3. The maximum corresponds to a temporal and spatial synchronisation between the two pulses in the BBO crystal, whereas the tails of the curve are obtained for non-zero delays between the pulses.

The duration of the gate is defined as the FWHM of the curve and is equal to 270 fs. It depends strongly on the angle θ between gating pulse and imaging pulse. Indeed, angle θ induces to a non-uniform overlap between the two pulses: when changing delay $\Delta\tau$ between the pulses, spatial overlap moves from one side of the imaging pulse to the other. Ideally, the gate duration may be reduced by using a very small angle θ. However, when angle θ is small, the two collinear SHG from the imaging pulse and the gating
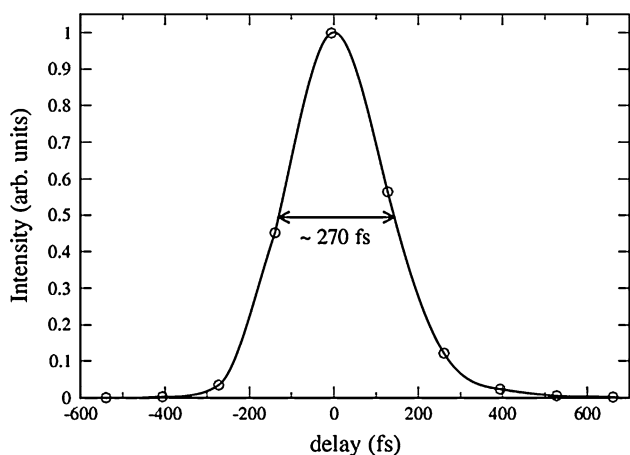
Fig. 3 Cross-correlation between imaging and gating pulses

pulse are close. The SF used to separate the collinear SHG from the non-collinear one and the camera must be located further from the BBO crystal. The value of θ is chosen as small as possible when the time gate duration measurement is only performed. By removing lenses L2, L3 and slit, and by replacing the camera by a power meter, it may be reduced to 2°. However, for the following experiments, where a high image resolution is expected, a compromise must be found concerning angle θ. Indeed, choosing a large θ allows to have the non-collinear SHG well separated from the collinear SHG generated by the crystal from the imaging and gating pulses. In this case, the overlap of the two pulses is not complete, leading to longer gate duration. Choosing a small angle θ allows shorter gate duration, but needs to move the camera away from the BBO crystal, inducing image degradation due to a long light propagation in air. Finally, it will be shown further that the choice of θ will not affect the temporal resolution of the time measurement, if the temporal dependence along the horizontal axis of the camera is taken into account.

3.2 Spatial resolution

To evaluate the spatial resolution of the overall system, the image of an US Air Force resolution chart including spatial
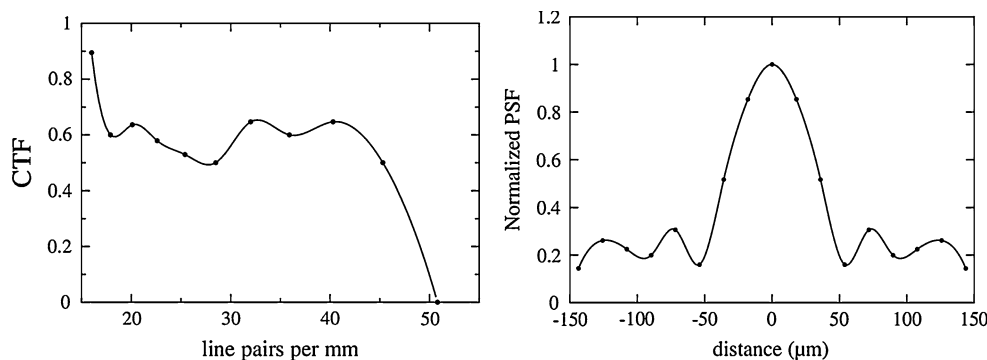
frequencies (from 0.25 to 645 lp/mm) is recorded on the camera. It allows to evaluate the modulation transfer function (MTF) of the gate for a range of spatial frequencies. For each group of the chart with spatial frequency $1/\delta x$, the contrast MTFδx is computed by $\mathrm{MTF}(\delta x) = \frac{I_{\max} - I_{\min}}{I_{\max} + I_{\min}}$ where $I_{\max}$ is the intensity of transparent lines and $I_{\min}$ is the intensity of opaque lines. Figure 4 shows the CTF (contrast transfer function) computed using the USAF test chart. Making the usual assumption that the CTF is close to the MTF, by computing its Fourier transform, the point-spread function (PSF) is deduced. The cut-off spatial frequency is 50 lp/mm and gives a resolution of 10 μm.

4 Spatio-temporal analysis of the transmitted light

4.1 Images of a glass fibre

In order to investigate the potential of the BBO crystal-based time gate, preliminary images have been recorded using a glass fibre as the object, without any other scattering medium. Figure 5a shows the non-gated image of a fibre (diameter = 240 μm). The two strips located at each side of the image is the background light, whereas the thin line at the centre corresponds to refracted light into the fibre. When the optical gate is operating, the ballistic light may be isolated (Fig. 5b). By adjusting the delay line, refractive light is isolated (Fig. 5c). The time delay difference between images Fig. 5b and c is $\Delta\tau = 380$ fs, according to the fibre diameter $d = 240$ μm and its refractive index $n \sim 1.5$.

4.2 Images of the liquid jet near the injector

The same set-up has been applied to a diesel jet visualisation. The measurements were carried out using a calibration liquid (ISO 4113) with properties similar to diesel fuel and having precisely controlled viscosity, density and surface tension specifications (Table 1). The injection pressure is 400 bars, the diameter of the nozzle hole is
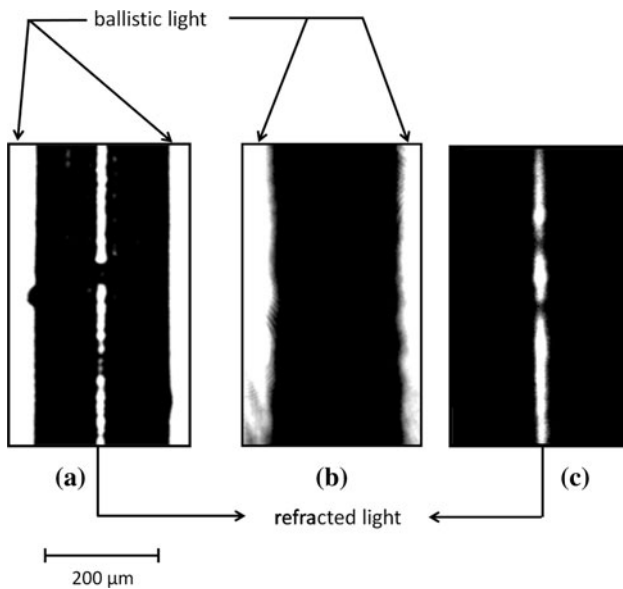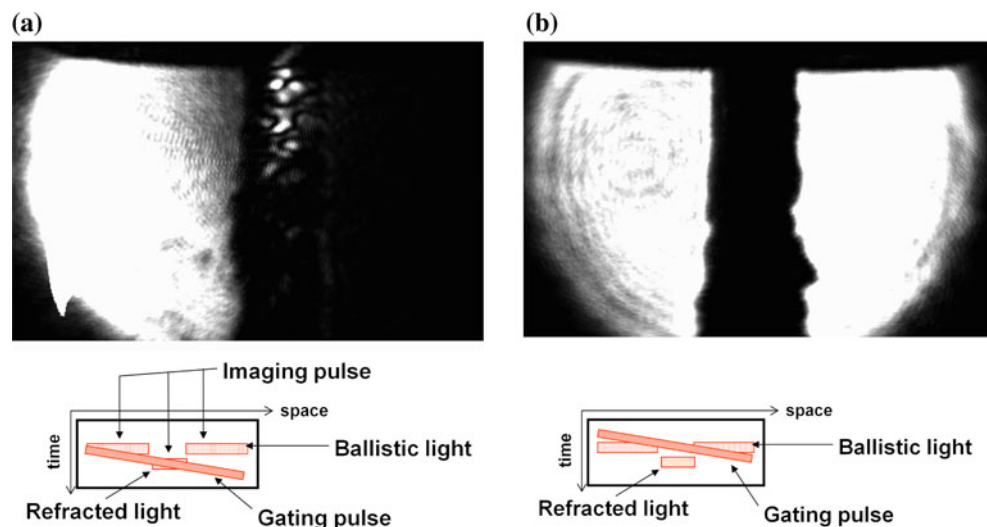
Fig. 4 MTF and PSF of the imaging system

Fig. 5 Image of a glass fibre without optical gate (**a**), for a delay allowing the selection of ballistic photons only (**b**) and for a delay allowing the selection of refracted light only (**c**)

Table 1 Thermophysical properties of ISO 4113 oil

Density	821 kg/m³
Viscosity	0.0032 kg/(m s)
Surface tension	0.02547 N/m

200 μm and the liquid is injected at atmospheric pressure and ambient temperature in a chamber. In the near field of the injector, the liquid roughly keeps the cylindrical shape of the injector hole. Observation of refractive light is expected at this location. Time-gated images are shown on Fig. 6, for two different delays between imaging and gating pulses. In both cases, the two pulses overlapped only partially, as a consequence of the angle θ, as schematically illustrated in the figure bottom. In Fig. 6a, the delay line is adjusted in such a way that the gating pulse and the ballistic component of the imaging pulse overlap in the left side of the image. The right side of the image, where the two pulses do not overlap, remains dark. In the middle part of the image, ballistic component does not overlap temporally with the gating pulse. But refractive light, which is time delayed due to the jet crossing, overlap with the gating pulse and is clearly visible on the image. Conversely, when the delay is adjusted to overlap the gating pulse and ballistic light at the right side of the image, refracted light is no more detected, and the liquid core appears to be completely dark (Fig. 6b). It must be noticed that if the image and gating pulses are symbolised by rectangles on the schemas of Fig. 6, their temporal and spatial shapes are approximately Gaussian, so that the tails of the pulses may be used to detect light at time delays smaller than the 270 fs duration, depending on the sensitivity of the detector. The time delay between image Fig. 6a and b is $\Delta\tau = 380$ fs. Knowing the refractive index of the injected liquid equal to 1.46, we can deduce an estimation of the jet diameter to about 250 μm. Cavitation inside the injector and of its influence on the atomisation process is a recent issue (Sou et al. 2011). Existence of refractive light at the exit of the injector leads to the conclusion that the fluid is completely liquid. Either if there is no cavitation or if cavitation occurs inside the injector, the gas phase is condensed at the exit.

4.3 Spatio-temporal diagrams

The qualitative description of the preceding images leads to the conclusion that a spatio-temporal study of the light after interaction with an object is possible by changing the delay

Fig. 6 Images of the liquid jet at the exit from injector hole for two different delays between image and pump pulses. The delay is adjusted on **a** to select refracted light at the centre of the jet, while it is adjusted on **b** to eliminate refracted light at the same location

$\Delta\tau$ between the gating pulse and the image pulse. Indeed, the image on the camera is the result of the spatio-temporal correlation of the gating pulse with the image pulse along the width of the BBO crystal. The complete model is complex, because of interdependent phenomena: the spatio-temporal profile of each pulse, the angle between beams, the slight translation of one pulse relatively to the other inside the crystal due to their different propagation directions, etc. However, a simplified interpretation of the image may be proposed by making some assumptions: (1) the image pulse and gating pulse are so short enough to be modelled by a time Dirac, (2) the magnification of the optical system is large, so that the image pulse may be considered uniform in space before interaction with any object, (3) the thickness of the BBO crystal is small, so that the shift of the gating pulse relatively to the image pulse is neglected, and (4) SHG light rays from the BBO are parallel.

With these assumptions, when the gating beam crosses the image beam somewhere in the crystal with angle θ between their propagation directions, a third pulse is produced, due to the SHG, at half angle. This intersection (point A on Fig. 7) produced a bright zone on the image recorded by the camera.

Now, if the gating pulse is affected by a delay $\Delta\tau$, the intersection point A is shifted to point B; then a shift ΔX appears on the camera screen. Following the scheme of Fig. 7, the relation between $\Delta\tau$ and ΔX leads to $\Delta\tau = \alpha\Delta X$, with $\alpha = 2\frac{\sin\theta_n/2}{c/n}$, where c is the speed of light in vacuum, θ_n is the angle between the two beams inside the crystal and n the refractive index of BBO crystal. Moreover, when intersection shifts from point A to point B, the intensity of

the bright zone varies proportionally with the intensity of the pump beam at point A or point B, modified by a coefficient due to the SHG process. Figure 8 shows the apparent intensity $I_0(\Delta\tau)$, computed as the maximum intensity of the image obtained on the camera, as a function of the delay $\Delta\tau$. It corresponds to the dotted line curve shown on the top of Fig. 7.

If now the imaging pulse, characterised here by a constant illumination of 100 fs duration, travels across a scattering medium like a spray, a temporal elongation of the image beam will occur due to scattering, refraction and diffraction of the light. The imaging pulse can no longer be approximated by a Dirac in time. The intensity distribution along the horizontal x axis of the camera is then the product of the gating pulse and the image pulse at different positions and times; it means that the time gate position is a function of the horizontal axis. Figure 9 shows the geometrical configuration corresponding to an overlap of the gating pulse and the elongated image pulse. Intensity of point A is proportional to the ballistic photons density multiplied by the gating pulse intensity at point A, whereas in B, intensity is proportional to the time delayed photons density multiplied by the gating pulse intensity at point B. On the camera, a pixel located at distance Δx along the horizontal axis from the known position of the ballistic photons gives an information on point B in terms of position x and delay τ. x and τ are easily deduced from Δx using Fig. 9:

$$x = \frac{\Delta x \cos\theta_n/2}{\cos\theta_n} \approx \Delta x \quad \text{and} \quad \tau = 2\frac{\Delta x \sin\theta_n/2}{c/n} \approx \alpha\Delta x \quad (1)$$

with the assumption that angle θ (and θ_n) between the beams is small. Because the intensity of the pump beam is not the same in A as in B, the apparent intensity of B on the camera must be corrected by $I_0(\Delta\tau)$, where $\Delta\tau$ is the time delay corresponding to distance BC (Fig. 9):

$$\Delta\tau = 2\frac{\Delta x \sin\theta_n/2}{c/n \times \cos\theta_n} \approx \alpha\Delta x \approx \tau \quad (2)$$
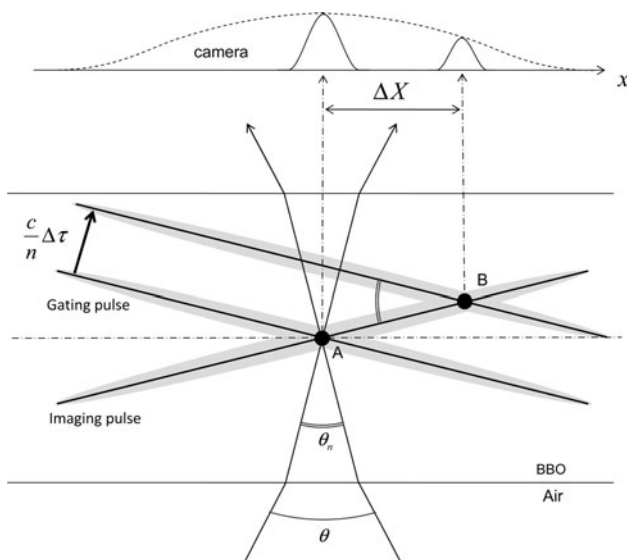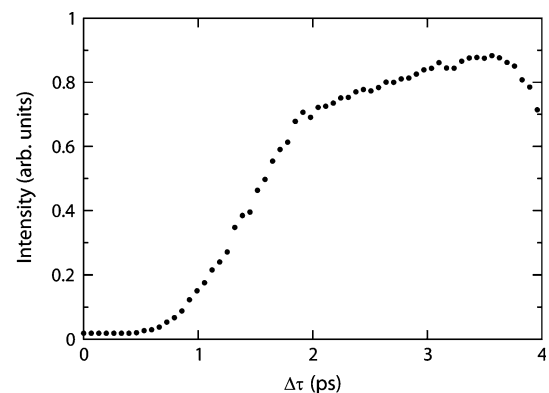

Fig. 7 Relation between the maximum of intensity recorded on camera and the delay. The propagation directions of both pulses are in the *horizontal* plane

Fig. 8 Apparent intensity versus the delay $\Delta\tau$

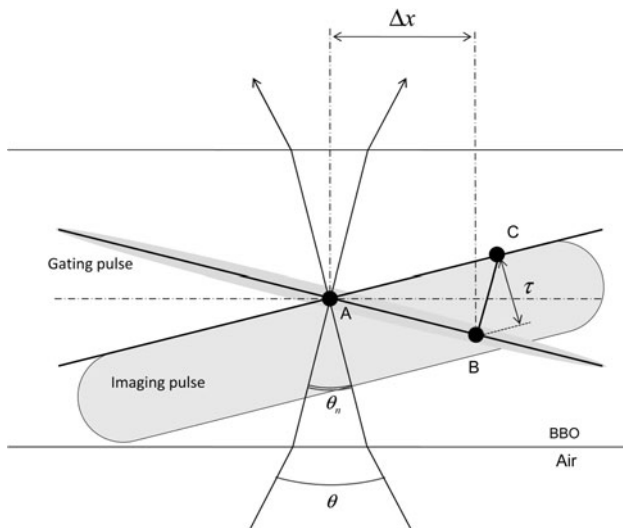**Fig. 9** Interaction between gating pulse and a time-elongated imaging pulse (after crossing an object). On the image, a pixel located at Δx corresponds to a time delay τ in respect to the ballistic photons

The preceding considerations may then be applied to the fibre. Images are recorded by varying the delay $\Delta\tau$ between gating pulse and image pulse. For each value $\Delta\tau$, 20 images of size $1{,}000 \times 1{,}000$ pixels are recorded from the CCD camera and an average image $I(\Delta\tau, x, y)$ is computed. Then, intensity $I(\Delta\tau, x)$ is obtained by averaging the pixels of each column y. The spatio-temporal diagrams $I(\Delta\tau, x)$ are shown on Fig. 10, in two cases: (a) without the fibre and (b) with the fibre. In Fig. 10a, the diagram is composed of ballistic photons. The bright area is oriented in accordance with the slope coefficient α previously introduced. The diagram of Fig. 10b shows a hole in the ballistic light, corresponding to the shadow of the fibre. As expected, refracted light undergoes a delay due to the fibre crossing. This diagram, which is a function of $I(\Delta\tau, x)$, may be straightened with the change of variables given by Eq. 1. In particular, the delay between the gating pulse and the image pulse becomes the time $t = \Delta\tau - \alpha\Delta x$. A normalisation by the gating pulse profile I_0 is then performed to
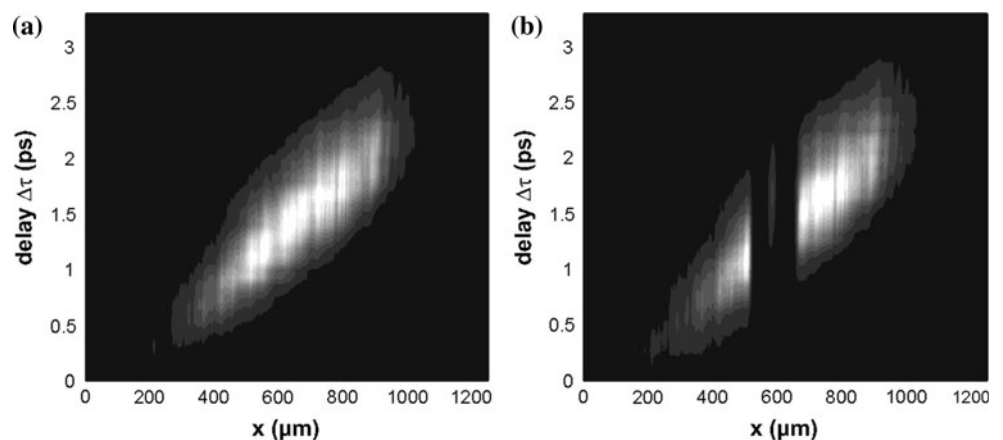
obtain a corrected spatio-temporal diagram presented in Fig. 11. It shows that with a suitable processing, the interaction of light with an object may be followed in time with the time gate based on a BBO crystal.

4.4 Spatio-temporal diagrams of the spray

The same process may be applied on the spray far from the nozzle. Figure 12 is a typical image at 5 mm from the nozzle, for one time delay, showing many bright spots corresponding to scattered light, which do not exist in the case of the fibre. The texture of this image evolves from the left to the right. As explained on Fig. 9, the horizontal axis includes space- and time-dependent information. The light recorded at the right part of the image corresponds to larger time delays than at the left part. Without the optical gate, the image would be completely uniform with randomly distributed bright spots.

This calibration is necessary to have a time reference. This calibration consists in determining coefficient α and to record an image without spray, which gives the location of the ballistic photons. Separation of the spatial contribution from the temporal one is impossible from a single image. If the object under study is static (like the glass fibre), it is possible to change the delay $\Delta\tau$ to reconstruct the complete spatio-temporal diagram. In the case of a liquid jet, only a statistical approach may be used.

Images are then recorded by varying the delay between the gating pulse and the image pulse. 100 images are recorded for each delay, and the same image processing than for the fibre is applied. Spatio-temporal diagrams $I(\Delta\tau - \alpha\Delta x, x)$ are shown on Fig. 13 in two cases: (a) without the spray, in order to determine coefficient α, and (b) with the spray. Cases (c) and (d) show corrected diagrams by using the change of variable of Eq. 1. One can observe that the optical gate is able to select the ballistic light.

Nevertheless, a detection of delayed light would be interesting in order to reconstruct the history of light
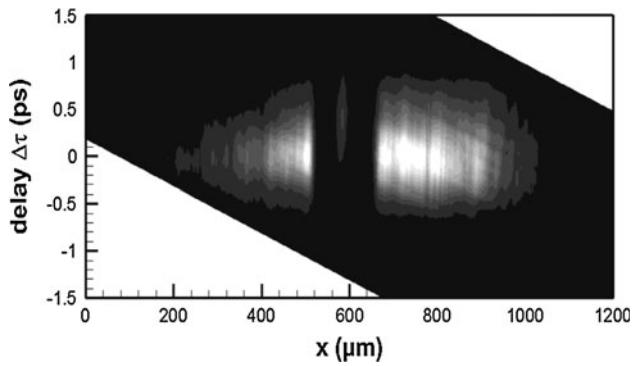
Fig. 10 Spatio-temporal diagrams of the ballistic light: **a** without the fibre and **b** with the glass fibre

Fig. 11 Corrected spatio-temporal diagram of light interaction with a glass fibre
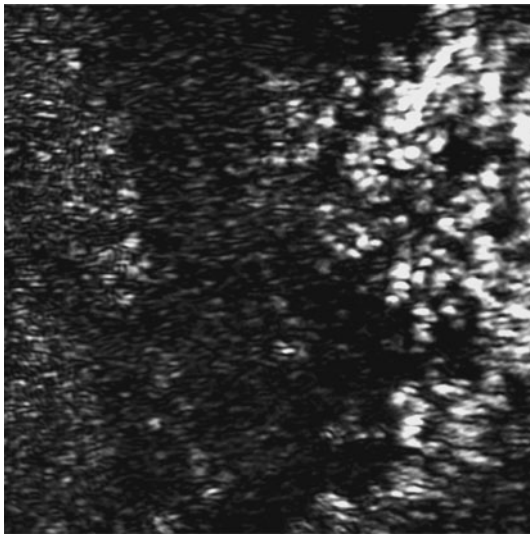
Fig. 12 A typical image of the spray far from the nozzle
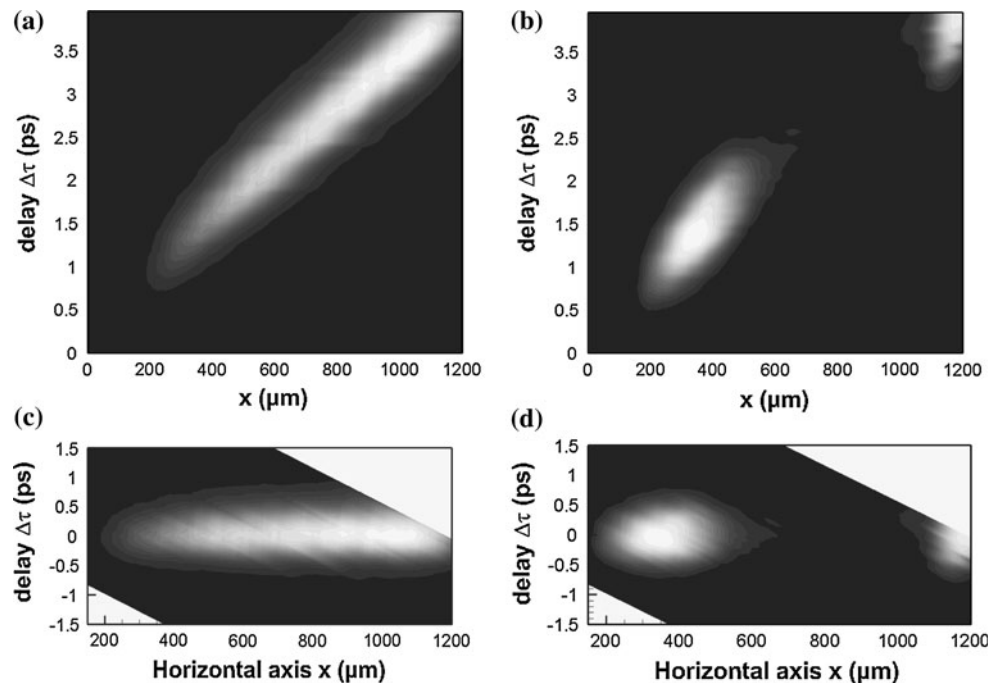
interaction with the spray. Due to the image averaging, and because of the limited dynamical range of the camera, no scattered light and also no ballistic one are visible on the spatio-temporal diagrams in the centre of the spray (Fig. 13d). Increasing the intensity of the imaging pulse is not a solution: a more intense imaging pulse would damage the camera. A vertical slit has been added in an intermediate image plane (see Fig. 2), in order to eliminate the sides of the image, which are too intense for the sensor. The intensity of the imaging pulse may then be increased, without the risk of camera damage, until obtaining a detectable level of the transmitted light through the spray.

We have used this last method at 200 μm from the nozzle, in a more dense part of the spray. Images are again recorded by changing delay $\Delta\tau$ between gating pulse and imaging pulse. An average is made over 100 images for each $\Delta\tau$, and spatio-temporal diagrams are computed and shown on Fig. 14. We have now transmitted light at the centre of the spray. A time shift is clearly observed between the reference diagram without spray (a) and the diagram with the spray (b). A delay of ~ 0.4 ps between the ballistic light and the transmitted light may be estimated by comparing these diagrams. Some light undergoes a shift of ~ 1 ps. These delays may be interpreted as an extra time due to multiple light scattering. In this case, the extra distance covered by the light in respect to the ballistic photons would correspond to ~ 12 mm, which is larger than the radius of the spray at 200 μm, as observed by shadowgraphy. A liquid core still exists at this distance from the nozzle.
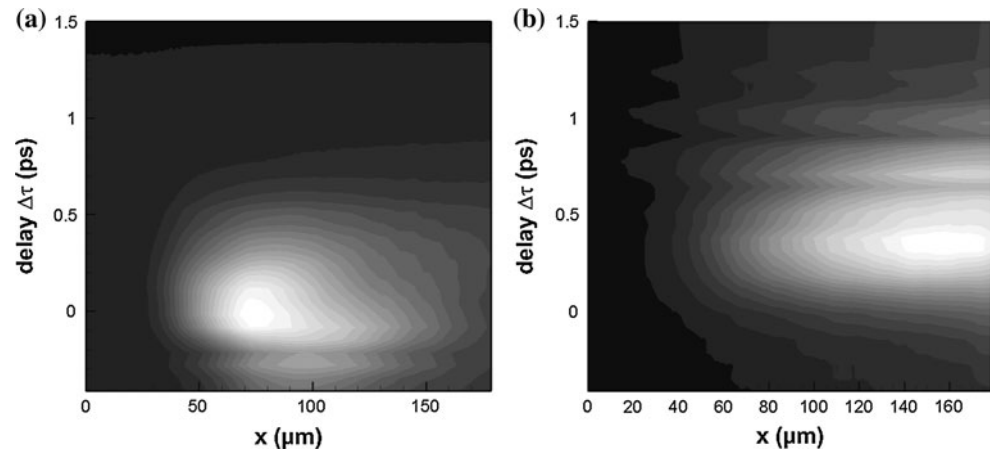
Fig. 13 Spatio-temporal diagrams of light at 5 mm from the nozzle: **a** without spray, **b** which has interacted with the spray. Subfigures **c** and **d** are modified by using the change of variable of Eq. 1

Fig. 14 Spatio-temporal diagrams of transmitted light at 200 µm from the nozzle: **a** without spray, **b** with the spray

5 Conclusion

The use of an optical gate based on SHG in a BBO crystal allows to reduce the temporal resolution in ballistic imaging, which is now compatible with the dimension of the spray resulting from a diesel injector. It has been shown that this gate is able to discriminate refractive light from ballistic light at the exit of the nozzle. A suitable image analysis may be used to perform a deconvolution between space and time on statistical series of spray images. An average time delay due to interaction of light and spray may then be estimated.

References

Abraham E, Bordenave E, Tsurumachi N, Jonusauskas G, Oberlé J, Rullière C, Mito A (2000) Real-time two-dimensional imaging in scattering media by use of a femtosecond Cr4 + : forsterite laser. Opt Lett 25:929–931

Berrocal E, Sedarsky DL, Paciaroni ME, Meglinski IV, Linne MA (2009) Laser light scattering in turbid media. Part II: spatial and temporal analysis of individual scattering orders via Monte Carlo simulation. Opt Exp 17:13792–13809

Berrocal E, Kristensson E, Hottenbach P, Grünefeld G and Aldén M (2011) Quantitative laser imaging of anon-reacting diesel spray using SLIPI. ILASS Americas, 23rd annual conference on liquid atomization and spray systems, Ventura, CA, USA

Calba C, Rozé C, Girasole T, Méès L (2006) Monte Carlo simulation of the interaction between an ultra-short pulse and a strongly scattering medium: the case of large particles. Opt Commun 265:373–382

Calba C, Méès L, Rozé C, Girasole T (2008) Ultra-short pulses propagation through a strongly scattering medium: simulation and experiments. J Opt Soc Am A 25(07):1541–1550

Farsiu S, Christofferson J, Eriksson B, Milanfar P, Friedlander B, Shakouri A, Nowak R (2007) Statistical detection and imaging of objects hidden in turbid media using ballistic photons. Appl Opt 46(23):5805–5822

Galland PA, Liang X, Wang L, Breisacher K, Liou L, Ho PP, Alfano RR (1995) Time-resolved optical imaging of jet sprays and droplets in highly scattering medium. Proc Am Soc Mech Eng HTD 321:585–588

Idlahcen S, Méès L, Rozé C, Girasole T, Blaisot JB (2009) Time gate, optical layout, and wavelength effects on ballistic imaging. J Opt Soc Am A 26:1995–2004

Kastengren AL, Powell CF, Wang YJ, Im KS and Wang J (2008) X-ray radiography measurements of diesel spray structure at engine-like ambient density. ILASS Americas, 21st annual conference on liquid atomization and spray systems, Orlando, FL, USA

Kristensson E, Berrocal E, Richter M, Aldén M (2010) Nanosecond structured laser illumination planar imaging for single-shot imaging of dense sprays. At Sprays 20:337–343

Kuditcher A, Hoover BG, Hehlen MP, Leith EN, Rand SC, Shih MP (2001) Cross-correlated harmonic imaging through scattering media. Appl Opt 40:45–51

Leick P, Grzeszik1 R, Arndt S, Wissel S (2011) Suppression of multiple scattering using structured light sheets—a first assessment for diesel and gasoline spray visualization. ILASS—Europe 2011, 24th European conference on liquid atomization and spray systems, Estoril, Portugal

Linne M, Paciaroni M, Halland T, Parker T (2006) Ballistic imaging of the near field in a diesel spray. Exp Fluids 40:836–846

Méès L, Gouesbet G, Gréhan G (2001) Time resolved scattering diagrams for a sphere illuminated by plane wave and focused short pulses. Opt Commun 194:59–65

Moon S, Liu Z, Gao J, Dufresne E, Fezzaa K and Wang J (2010) Ultrafast X-ray phase-contrast imaging of high-speed fuel sprays from a two-hole Diesel nozzle. ILASS Americas, 22nd annual conference on liquid atomization and spray systems, Cincinnati, OH, USA

Paciaroni M, Hall T, Delpanque JP, Parker T, Linne M (2006) Single-shot two-dimensional ballistic imaging of the liquid core in an atomizing spray. At Sprays 16:51–59

Sbanski O, Roman VE, Kiefer W, Popp J (2000) Elastic light scattering from single microparticles on a femtosecond time scale. J Opt Soc Am A 17(2):313–319

Schmidt JB, Schaefer ZD, Meyer TR, Roy S, Danczyk SA, Gord JR (2009) Ultrafast time-gated ballistic-photon imaging and shadowgraphy in optically dense rocket sprays. Appl Opt 48:B137–B144

Sedarsky D, Berrocal E, Linne M (2011) Quantitative image contrast enhancement in time-gated transillumination of scattering media. Opt Exp 19:1866–1883

Sou A, Pratama RH, Ohashi R, Sugimura R (2011) Cavitation in a nozzle with asymmetric inflow and its effects on liquid jet. ILASS—Europe 2011, 24th European conference on liquid atomization and spray systems, Estoril, Portugal

Wang L, Ho PP, Liu F, Zhang G, Alfano RR (1991) Ballistic 2-D imaging through scattering walls using an ultrafast optical Kerr gate. Science 253:769–771